

Universität des Saarlandes



Fachrichtung 6.1 – Mathematik

Preprint Nr. 237

**Adaptive Continuous-Scale Morphology  
for Matrix Fields**

Bernhard Burgeth, Luis Pizarro,  
Michael Breuß and Joachim Weickert

Saarbrücken 2009



## Adaptive Continuous-Scale Morphology for Matrix Fields

**Bernhard Burgeth**

Saarland University  
Department of Mathematics  
P.O. Box 15 11 50  
66041 Saarbrücken  
Germany  
burgeth@math.uni-sb.de

**Luis Pizarro**

Saarland University  
Department of Mathematics  
P.O. Box 15 11 50  
66041 Saarbrücken  
Germany  
pizarro@mia.uni-saarland.de

**Michael Breuß**

Saarland University  
Department of Mathematics  
P.O. Box 15 11 50  
66041 Saarbrücken  
Germany  
breuss@mia.uni-saarland.de

**Joachim Weickert**

Saarland University  
Department of Mathematics  
P.O. Box 15 11 50  
66041 Saarbrücken  
Germany  
weickert@mia.uni-saarland.de

Edited by  
FR 6.1 – Mathematik  
Universität des Saarlandes  
Postfach 15 11 50  
66041 Saarbrücken  
Germany

Fax: + 49 681 302 4443  
e-Mail: [preprint@math.uni-sb.de](mailto:preprint@math.uni-sb.de)  
WWW: <http://www.math.uni-sb.de/>

## Abstract

In this article we consider adaptive, PDE-driven morphological operations for 3D matrix fields arising e.g. in diffusion tensor magnetic resonance imaging (DT-MRI). The anisotropic evolution is steered by a matrix constructed from a structure tensor for matrix valued data. An important novelty is an intrinsically one-dimensional directional variant of the matrix-valued upwind schemes such as the Rouy-Tourin scheme. It enables our method to complete or enhance anisotropic structures effectively. A special advantage of our approach is that upwind schemes are utilised only in their basic one-dimensional version. No higher dimensional variants of the schemes themselves are required. Experiments with synthetic and real-world data substantiate the gap-closing and line-completing properties of the proposed method.

**Keywords.**Mathematical Morphology; PDEs; DT-MRI; Tensor field; Dilation; Erosion

## 1 Introduction

One of the primary tasks of mathematical morphology is the enhancement and extraction of shape information from image objects. This task is successfully tackled with a multitude of morphological operations based on the fundamental dilation and erosion processes. Dilation and erosion can be realised in a set-theoretic or ordering based framework, see e.g. [29, 40, 30, 41, 42, 44], but it may also be implemented within the context of partial differential equations (PDE) [1, 3, 12, 38, 45] and their numerical solution schemes (see [10] as well as the extensive list of literature cited there). The PDE-based approach is conceptually attractive since it allows for digital scalability and even adaptivity of the represented structuring element. This versatility was exploited, for example in [9] and [11] to create adaptive, PDE-based dilation processes for grey value images. In [15] the idea of morphological adaptivity has been transferred to the setting of matrix fields utilising the operator-algebraic framework proposed in [18]. Matrix fields offer the opportunity of describing anisotropy in physical measurements and in image processing models see [50],[28] for an overview. In diffusion tensor magnetic resonance imaging (DT-MRI), for example, information about the diffusive properties of water molecules is captured in symmetric positive definite matrices. The corresponding matrix field reflects the structure of the tissue under examination. The goal of [15] was to enhance line-like and coherent structures in DT-MRI data. In this article we propose a concept for PDE-based adaptive

morphology for matrix fields, involving directional derivatives in the formulation of the PDE-based dilation and erosion processes. In contrast to the approach in [15] and as a 3D-extension of the work in [35] the numerical realisation employed in this article takes advantage of the accurate calculation of directional derivatives that relies on tri-linear interpolation.

We will start from a scalar adaptive formulation for  $d$ -dimensional data  $u$  in form of the dilation PDE

$$\partial_t u = \|M(u) \cdot \nabla u\| \quad (1)$$

with a data dependent, symmetric, positive semidefinite  $d \times d$ -matrix  $M = M(u)$ . When considering three-dimensional matrix-fields, for example, in DT-MRI data sets ( $d = 3$ ) one has

$$M = \begin{pmatrix} a_{11} & a_{12} & a_{13} \\ a_{21} & a_{22} & a_{23} \\ a_{31} & a_{32} & a_{33} \end{pmatrix} = \begin{pmatrix} \|(a_{11}, a_{11}, a_{13})\| \nu^\top \\ \|(a_{21}, a_{21}, a_{23})\| \mu^\top \\ \|(a_{31}, a_{31}, a_{33})\| \eta^\top \end{pmatrix} \quad (2)$$

with unit vectors  $\nu, \mu$ , and  $\eta$  where, e.g.

$$\nu = \frac{1}{\|(a_{11}, a_{12}, a_{13})\|} \begin{pmatrix} a_{11} \\ a_{12} \\ a_{13} \end{pmatrix} \quad (3)$$

This turns (1) into

$$\begin{aligned} \partial_t u &= \left( (a_{11} \partial_x u + a_{12} \partial_y u + a_{13} \partial_z u)^2 \right. \\ &\quad + (a_{21} \partial_x u + a_{22} \partial_y u + a_{23} \partial_z u)^2 \\ &\quad \left. + (a_{31} \partial_x u + a_{32} \partial_y u + a_{33} \partial_z u)^2 \right)^{\frac{1}{2}} \end{aligned} \quad (4)$$

$$\begin{aligned} &= \left( \|(a_{11}, a_{12}, a_{13})\|^2 (\partial_\nu u)^2 \right. \\ &\quad + \|(a_{21}, a_{22}, a_{23})\|^2 (\partial_\mu u)^2 \\ &\quad \left. + \|(a_{31}, a_{32}, a_{33})\|^2 (\partial_\eta u)^2 \right)^{\frac{1}{2}} \end{aligned} \quad (5)$$

In [15] the partial derivatives  $\partial_x u$ ,  $\partial_y u$ , and  $\partial_z u$  in (4) were approximated with the standard Rouy-Tourin scheme [37] in its two-dimensional version to obtain a directional derivative. However, in [35] the directional derivatives necessary for the steering process were realised directly by means of equation (5) with better results than in [15]. Hence it is decisive for our approach to implement the directional derivatives  $\partial_\nu u$ ,  $\partial_\mu u$ , and  $\partial_\eta u$  in (5) via a directional version of the Rouy-Tourin scheme as an upwind scheme suitable for

the numerical solution of a transport equation (5). As it will be explained in Section 4 an important feature of the proposed approach is the fact that the upwind schemes are employed only in their simplest one-dimensional variant regardless of the dimensionality of the data set. No specially designed higher-dimensional versions or operator splitting methods have to be engaged.

This opens the path for using a high resolution method such as the flux-corrected-transport (FCT) scheme of [10] for which its 3D-version is not easily obtained in adaptive form in the setting of matrix fields. In total the novel features over [15] and [35] are the realisation of higher morphological operators based on an adaptive directional version of the FCT scheme in three spatial dimensions.

Equation (1) describes a dilation with an ellipsoidal structuring element since an application of the mapping  $(x, y, z)^\top \mapsto M \cdot (x, y, z)^\top$  transforms a sphere centered around the origin into an ellipsoid. The necessary directional information of the evolving  $u$  contained in the matrix  $M(u)$  may be derived from the so-called structure tensor. The *structure tensor*, dating back to [23, 5], allows to extract directional information from an image. It is given by

$$S_\rho(u(x)) := G_\rho * (\nabla u(x) \cdot (\nabla u(x))^\top) \quad (6)$$

$$= (G_\rho * (\partial_{x_i} u(x) \cdot \partial_{x_j} u(x)))_{i,j=1,\dots,d} \quad (7)$$

Here  $G_\rho*$  indicates a convolution with a Gaussian of standard deviation  $\rho$ . For more details the reader is referred to [4] and the literature cited therein. In [13, 22] Di Zenzo's approach [21] to construct a structure tensor for multi-channel images has been extended to matrix fields yielding a *standard structure tensor*

$$J_\rho(U(x)) := \sum_{i,j=1}^m S_\rho(U_{i,j}(x)) \quad (8)$$

with matrix entries  $U_{i,j}$ ,  $i, j = 1, \dots, m$ . This tensor is a special case of the *full structure tensor concept* for matrix fields as proposed in [19]. We will review this full structure concept in Section 2.

The article is structured as follows: In Section 2 we briefly give an account of basic notions of matrix analysis needed to establish a matrix-valued PDE for an adaptively steered morphological dilation process. We introduce the steering tensor that guides the dilation process adaptively in Section 3. It is explained how the numerical FCT scheme is turned into a directional variant that can be used on matrix fields in Section 4. Section 5 contains the definitions of the morphological operators we are going to extend in their directional versions to matrix fields. An evaluation of the performance of our approach to adaptive morphology for matrix fields is the subject of Section 6. The remarks in Section 7 conclude this article.

## 2 Matrix Analysis and an Extended Structure Tensor Concept

This section contains the key definitions for the formulation of matrix-valued PDEs. For a more detailed exposition the reader is referred to [18].

A matrix field is considered as a mapping  $U : \Omega \subset \mathbb{R}^d \longrightarrow \text{Sym}_m(\mathbb{R})$  from a  $d$ -dimensional image domain into the set of symmetric  $m \times m$ -matrices with real entries,  $U(x) = (U_{p,q}(x))_{p,q=1,\dots,m}$ . The set of positive (semi-) definite matrices, denoted by  $\text{Sym}_m^{++}(\mathbb{R})$  (resp.,  $\text{Sym}_m^+(\mathbb{R})$ ), consists of all symmetric matrices  $A$  with  $\langle v, Av \rangle := v^\top Av > 0$  (resp.,  $\geq 0$ ) for  $v \in \mathbb{R}^m \setminus \{0\}$ . This set is of special interest since DT-MRI produces data with this property. Note that at each point  $x$  the matrix  $U(x)$  of a field of symmetric matrices can be diagonalised yielding  $U(x) = V(x)^\top D(x)V(x)$ , where  $V(x)$  is a orthogonal matrix, while  $D(x)$  is a diagonal matrix. In the sequel we will denote  $m \times m$ -diagonal matrices with entries  $\lambda_1, \dots, \lambda_m \in \mathbb{R}$  from left to right simply by  $\text{diag}(\lambda_i)$ .

The extension of a function  $h : \mathbb{R} \longrightarrow \mathbb{R}$  to  $\text{Sym}_m(\mathbb{R})$  is standard [26]: With a slight abuse of notation we set  $h(U) := V^\top \text{diag}(h(\lambda_1), \dots, h(\lambda_m))V \in \text{Sym}_m^+(\mathbb{R})$ ,  $h$  denoting now a function acting on matrices as well. Specifying  $h(s) = |s|, s \in \mathbb{R}$  as the absolute value function leads to the absolute value  $|A| \in \text{Sym}_m^+(\mathbb{R})$  of a matrix  $A$ . It is natural to define the partial derivative for matrix fields *componentwise*:

$$\bar{\partial}_\omega U = (\partial_\omega U_{p,q})_{p,q=1,\dots,m} \quad (9)$$

where  $\omega \in \{t, x_1, \dots, x_d\}$ , that is,  $\bar{\partial}_\omega$  stands for a spatial or temporal derivative. Viewing a matrix as a tensor (of second order), its gradient would be a third order tensor according to the rules of differential geometry. However, we adopt a more operator-algebraic point of view by defining the *generalised gradient*  $\bar{\nabla}U(x)$  at a voxel  $x = (x_1, \dots, x_d)$  by

$$\bar{\nabla}U(x) := (\bar{\partial}_{x_1}U(x), \dots, \bar{\partial}_{x_d}U(x))^\top \quad (10)$$

which is an element of  $(\text{Sym}_m(\mathbb{R}))^d$ , in close analogy to the scalar setting where  $\nabla u(x) \in \mathbb{R}^d$ . For  $W \in (\text{Sym}_m(\mathbb{R}))^d$  we set  $|W|_p := \sqrt[p]{|W_1|^p + \dots + |W_d|^p}$  for  $0 < p < +\infty$ . It results in a positive semidefinite matrix from  $\text{Sym}_m^+(\mathbb{R})$ , the direct counterpart of a nonnegative real number as the length of a vector in  $\mathbb{R}^d$ .

There will be the need for a symmetric multiplication of symmetric matrices. We opt for the so-called *Jordan product*  $A \bullet B := \frac{1}{2}(AB + BA)$ . It produces a symmetric matrix, and it is commutative but neither associative nor distributive.

Furthermore, for later use in numerical schemes we have to clarify the notion of maximum and minimum of two symmetric matrices  $A, B$ . In direct analogy with relations known to be valid for real numbers one defines [16]:

$$\max(A, B) = \frac{1}{2}(A + B + |A - B|) \quad (11)$$

$$\min(A, B) = \frac{1}{2}(A + B - |A - B|) \quad (12)$$

where  $|F|$  stands for the absolute value of the matrix  $F$ .

With this at our disposal we formulate the matrix-valued counterpart of (1) as

$$\bar{\partial}_t U = |\bar{M}(U) \bullet \bar{\nabla} U|_2 \quad (13)$$

with an initial matrix field  $F(x) = U(x, 0)$ . Here  $\bar{M}(U)$  denotes a symmetric  $md \times md$ -block matrix with  $d^2$  blocks of size  $m \times m$  that is multiplied block-wise with  $\bar{\nabla} U$  employing the Jordan product " $\bullet$ ". Note that  $|\cdot|_2$  stands for the length of  $\bar{M}(U) \bullet \bar{\nabla} U$  in the matrix valued sense. The construction of  $\bar{M}(U)$  is detailed in Section 3 and relies on the full structure tensor.

The full structure tensor  $\bar{\mathcal{S}}_L$  for matrix fields as defined in [19] reads

$$\bar{\mathcal{S}}_L(U) := G_\rho * (\bar{\nabla} U \cdot (\bar{\nabla} U)^\top) \quad (14)$$

$$= (G_\rho * (\bar{\partial}_{x_i} U \cdot \bar{\partial}_{x_j} U))_{i,j=1,\dots,d} \quad (15)$$

with  $G_\rho *$  indicating a convolution with a Gaussian of standard deviation  $\rho$ .  $\bar{\mathcal{S}}_L(U(x))$  is a symmetric  $md \times md$ -block matrix with  $d^2$  blocks of size  $m \times m$ ,  $\bar{\mathcal{S}}_L(U(x)) \in \text{Sym}_d(\text{Sym}_m(\mathbb{R})) = \text{Sym}_{md}(\mathbb{R})$ . Typically for the 3D medical DT-MRI data one has  $d = 3$  and  $m = 3$ , yielding a  $9 \times 9$ -matrix  $\bar{\mathcal{S}}_L$ . It can be diagonalised as  $\bar{\mathcal{S}}_L(U) = \sum_{k=1}^{md} \lambda_k w_k w_k^\top$  with real eigenvalues  $\lambda_k$  (w.l.o.g. arranged in decreasing order) and an orthonormal basis  $\{w_k\}_{k=1,\dots,md}$  of  $\mathbb{R}^{md}$ . In order to extract useful  $d$ -dimensional directional information,  $\bar{\mathcal{S}}_L(U) \in \text{Sym}_{md}(\mathbb{R})$  is reduced to a structure tensor  $S(U) \in \text{Sym}_d(\mathbb{R})$  in a generalised projection step [19] using the block operator matrix  $\text{Tr}_A := \text{diag}(\text{tr}_A, \dots, \text{tr}_A)$  containing the trace operation. We set  $\text{Tr} := \text{Tr}_{I_m}$  where  $I_m$  denotes the  $m \times m$  unit matrix. This operator matrix acts on elements of the space  $(\text{Sym}_m(\mathbb{R}))^d$  as well as on block matrices via formal block-wise matrix multiplication,

$$\begin{pmatrix} \text{tr}_A & \cdots & 0 \\ \vdots & \ddots & \vdots \\ 0 & \cdots & \text{tr}_A \end{pmatrix} \begin{pmatrix} M_{11} & \cdots & M_{1d} \\ \vdots & \ddots & \vdots \\ M_{d1} & \cdots & M_{dd} \end{pmatrix} = \begin{pmatrix} \text{tr}_A(M_{11}) & \cdots & \text{tr}_A(M_{1d}) \\ \vdots & \ddots & \vdots \\ \text{tr}_A(M_{d1}) & \cdots & \text{tr}_A(M_{dd}) \end{pmatrix}, \quad (16)$$

provided that the square blocks  $M_{ij}$  have the same size as  $A$ . The projection that is conveyed by the reduction process condenses the directional information contained in  $\overline{\mathcal{S}}_L(U)$ , for a more detailed reasoning we must refer the reader to [19] for the sake of brevity. The reduction operation is accompanied by an extension operation: The  $I_m$ -extension is the mapping from  $\text{Sym}_d(\mathbb{R})$  to  $\text{Sym}_{md}(\mathbb{R})$  conveyed by the *Kronecker product*  $\otimes$ :

$$\begin{pmatrix} v_{11} & \cdots & v_{1d} \\ \vdots & \ddots & \vdots \\ v_{d1} & \cdots & v_{dd} \end{pmatrix} \mapsto \begin{pmatrix} v_{11} & \cdots & v_{1d} \\ \vdots & \ddots & \vdots \\ v_{d1} & \cdots & v_{dd} \end{pmatrix} \otimes I_m \quad (17)$$

$$:= \begin{pmatrix} v_{11}I_m & \cdots & v_{1d}I_m \\ \vdots & \ddots & \vdots \\ v_{d1}I_m & \cdots & v_{dd}I_m \end{pmatrix}. \quad (18)$$

This resizing step renders a proper matrix-vector multiplication with the large generalised gradient  $\overline{\nabla}U(x)$  possible. By specifying the matrix  $A$  in (16) one may invoke a priori knowledge into the direction estimation [19]. The research on these structure-tensor concepts has been initiated by [49, 13]. The approaches to matrix field regularisation suggested in [20] are based on differential geometric considerations. Comprehensive survey articles on the analysis of matrix fields using various techniques can be found in [50].

### 3 Steering Matrix $\overline{M}(U)$ for Matrix Fields

With these notions we are in the position to propose the steering matrix  $\overline{M}$  in the adaptive dilation process for matrix fields. We proceed in four steps:

1. The matrix field  $\mathbb{R}^d \ni x \mapsto U(x)$  provides us with a module field of generalised gradients  $\overline{\nabla}U(x)$  from which we construct the generalised structure tensor  $\overline{\mathcal{S}}_L(U(x))$  possibly with a certain integration scale  $\rho$ . This step corresponds exactly to the scalar case.
2. We infer  $d$ -dimensional directional information by reducing  $\overline{\mathcal{S}}_L(U(x))$  with  $\text{tr}_A$  with the help of the block operator matrix given in (16). This leads to a symmetric  $d \times d$ -matrix  $S$ , for example  $S = J_\rho$  if  $A = I_m$ :

$$S(x) := \text{Tr}_A(\overline{\mathcal{S}}_L(U(x))). \quad (19)$$

3. The symmetric  $d \times d$ -matrix  $S$  is spectrally decomposed, and the following mapping is applied:

$$H : \begin{cases} \mathbb{R}_+^d & \longrightarrow \mathbb{R}^d \\ (\lambda_1, \dots, \lambda_d) & \longmapsto \frac{1}{\sum_{i=1}^d \lambda_i} (c_1 \lambda_1, \dots, c_d \lambda_d) \end{cases} \quad (20)$$

where  $c = (c_1, \dots, c_d)$  is a vector with nonnegative entries. With the choice of the vector  $c$  we select the eigendirection in which the process is steered. For instance, specifying  $c_1 = \dots = c_{d-1} = k$  and  $c_d = K \gg k$  one obtains an ellipsoid associated with the matrix  $M$  which is flipped if compared with  $S$ . Depending on the choice of  $K$  it can be more excentric than the one accompanying  $S$ .  $H$  applied to  $S$  yields the steering matrix  $M$ ,

$$M := H(S). \quad (21)$$

4. Finally we enlarge the  $d \times d$ -matrix  $M$  to a  $md \times md$ -matrix  $\overline{M}$  by the extension operation

$$\overline{M} = M \otimes I_m. \quad (22)$$

## 4 Directional Numerical Schemes in the Matrix-Valued Setting

For the numerical solution of nonlinear PDEs governing the dilation or erosion processes first-order finite difference methods such as the *Osher-Sethian scheme* [31, 34, 43] and the *Rouy-Tourin method* [37, 46] are popular choices. They are capable of correctly capturing propagating shocks, however, at the price of introducing some dissipation and blurring of edges. A remedy is provided by the flux-corrected transport (FCT) scheme introduced in [10] for scalar-valued morphology. By construction it utilises a first order-scheme as a primary step and then performs a careful correction of the introduced dissipation in a second step. In the subsequent two sections we sketch the *directional* versions of the Rouy-Tourin scheme and the FCT scheme with their extensions to the matrix-valued setting.

### 4.1 Directional form of the Rouy-Tourin scheme

The first-order finite difference method of *Rouy and Tourin* [37] may be used to solve the scalar PDE (5) in the *isotropic* case with  $M = I_d$ . Let us denote by  $u_{i,j,k}^n$  the grey value of a scalar 3D image data set  $u$  at the pixel centered in  $(ih_x, jh_y, kh_z) \in \mathbb{R}^3$  at the time-level  $n\tau$  of the evolution. Furthermore, we employ standard forward, backward, and central difference operators, i.e.,

$$D_+^x u_{i,j,k}^n := u_{i+1,j,k}^n - u_{i,j,k}^n \quad (23)$$

and

$$D_-^x u_{i,j,k}^n := u_{i,j,k}^n - u_{i-1,j,k}^n \quad (24)$$

and finally

$$D_c^x u_{i,j,k}^n := (u_{i+1,j,k}^n - u_{i-1,j,k}^n) / 2 \quad (25)$$

here in  $x$ -, but analogously in  $y$ - and  $z$ -direction as well. The Rouy-Tourin method utilises an *upwind approximation* in the pixel  $(ih_x, jh_y, kh_z)$  of the partial derivative  $u_x$  (and analogously  $u_y, u_z$ ):

$$u_x \approx \frac{1}{h_x} \max \left( \max \left( -D_-^x u_{i,j,k}^n, 0 \right), \max \left( D_+^x u_{i,j,k}^n, 0 \right) \right). \quad (26)$$

For a unit vector  $\nu = (\nu_1, \nu_2, \nu_3)^\top$  the directional derivative  $\partial_\nu u$  of  $u$  may be approximated by  $\partial_\nu u = \langle \nu, \nabla u \rangle = \nu_1 \partial_x u + \nu_2 \partial_y u + \nu_3 \partial_z u$ . Hence it is close at hand to approximate numerically equation (4) directly. However, this favours mass transport along the directions of the  $x$ -,  $y$ -, and  $z$ -axis leading to a poor representation of the directional derivative. Instead we take advantage of equation (5) in this article and propose an alternative involving an interpolated function value  $u_{i+\nu_1, j+\nu_2, k+\nu_3}$  defined by the subsequent tri-linear <sup>1</sup> approximation (27):

$$\begin{aligned} u_{i+\nu_1, j+\nu_2, k+\nu_3} &= u_{i,j,k} \cdot (1 - h_x |\nu_1|) \cdot (1 - h_y |\nu_2|) \cdot (1 - h_z |\nu_3|) \\ &+ u_{i+\text{sign}(\nu_1), j, k} \cdot h_x |\nu_1| \cdot (1 - h_y |\nu_2|) \cdot (1 - h_z |\nu_3|) \\ &+ u_{i, j+\text{sign}(\nu_2), k} \cdot (1 - h_x |\nu_1|) \cdot h_y |\nu_2| \cdot (1 - h_z |\nu_3|) \\ &+ u_{i+\text{sign}(\nu_1), j+\text{sign}(\nu_2), k} \cdot h_x |\nu_1| \cdot h_y |\nu_2| \cdot (1 - h_z |\nu_3|) \\ &+ u_{i, j, k+\text{sign}(\nu_3)} \cdot (1 - h_x |\nu_1|) \cdot (1 - h_y |\nu_2|) \cdot h_z |\nu_3| \\ &+ u_{i+\text{sign}(\nu_1), j, k+\text{sign}(\nu_3)} \cdot h_x |\nu_1| \cdot (1 - h_y |\nu_2|) \cdot h_z |\nu_3| \\ &+ u_{i, j+\text{sign}(\nu_2), k+\text{sign}(\nu_3)} \cdot (1 - h_x |\nu_1|) \cdot h_y |\nu_2| \cdot h_z |\nu_3| \\ &+ u_{i+\text{sign}(\nu_1), j+\text{sign}(\nu_2), k+\text{sign}(\nu_3)} \cdot h_x |\nu_1| \cdot h_y |\nu_2| \cdot h_z |\nu_3|. \end{aligned} \quad (27)$$

This leads to forward and backward difference operators in the direction of  $\nu$  with  $\|\nu\| = \sqrt{\nu_1^2 + \nu_2^2 + \nu_3^2} = 1$ :

$$D_+^\nu u_{i,j,k}^n := u_{i+\nu_1, j+\nu_2, k+\nu_3}^n - u_{i,j,k}^n \quad (28)$$

$$D_-^\nu u_{i,j,k}^n := u_{i,j,k}^n - u_{i-\nu_1, j-\nu_2, k-\nu_3}^n \quad (29)$$

and to a direct approximation of the directional derivative

$$\begin{aligned} \partial_\nu u &= u_\nu \\ &\approx \frac{1}{h} \max \left( \max \left( -D_-^\nu u_{i,j,k}^n, 0 \right), \max \left( D_+^\nu u_{i,j,k}^n, 0 \right) \right) \end{aligned} \quad (30)$$

---

<sup>1</sup>For the sake of efficiency we use tri-linear interpolation, although higher order alternatives such as tri-cubic or spline interpolation can be employed as well.

where  $h := \min(h_x, h_y, h_z)$ . Furthermore, the resulting approximation of the directional derivatives is also consistent: tri-linear approximation implies

$$u_{i+\nu_1, j+\nu_2, k+\nu_3} = u((i + \nu_1)h_x, (j + \nu_2)h_y, (k + \nu_3)h_z) + \mathcal{O}(\max(h_x, h_y, h_z)), \quad (31)$$

and hence we have

$$\begin{aligned} & \frac{1}{h} D_+^\nu u_{i,j,k} \\ &= \frac{1}{h} (u((i + \nu_1)h_x, (j + \nu_2)h_y, (k + \nu_3)h_z) - u(ih_x, jh_y, kh_z)) \\ & \quad + \mathcal{O}(\max(h_x, h_y, h_z)) \end{aligned} \quad (32)$$

$$= u_\nu + \mathcal{O}(\max(h_x, h_y, h_z)). \quad (33)$$

Analogous reasoning applies to  $D_-^\nu u_{i,j,k}$ . With the calculus concept presented in Section 2 it is now straightforward to define one-sided directional differences in  $\nu$ -direction for fields of  $m \times m$ -matrices:

$$\begin{aligned} & D_+^\nu U^n(ih_x, jh_y, kh_z) \\ &:= U^n((i + \nu_1)h_x, (j + \nu_2)h_y, (k + \nu_3)h_z) - U^n(ih_x, jh_y, kh_z) \end{aligned} \quad (34)$$

$$\begin{aligned} & D_-^\nu U^n(ih_x, jh_y, kh_z) \\ &:= U^n(ih_x, jh_y, kh_z) - U^n((i - \nu_1)h_x, (j - \nu_2)h_y, (k - \nu_3)h_z) \end{aligned} \quad (35)$$

where  $D_+^\nu U^n, D_-^\nu U^n \in \text{Sym}_m(\mathbb{R})$ . In order to avoid confusion with the subscript notation for matrix components we wrote  $U(ih_x, jh_y, kh_z)$  to indicate the (matrix-) value of the matrix field evaluated at the voxel centred at  $(ih_x, jh_y, kh_z) \in \mathbb{R}^3$ . The directions  $\mu$  and  $\eta$  are treated accordingly. The notion of supremum and infimum of two matrices – as needed in a matrix variant of Rouy-Tourin – has been provided in Section 2 as well. Hence, having these generalisations at our disposal a directionally adaptive version of the Rouy-Tourin scheme is available now in the setting of matrix fields simply by replacing grey values  $u_{i,j,k}^n$  by matrices  $U^n(ih_x, jh_y, kh_z)$  and utilising the directional derivative approximations.

## 4.2 Directional FCT scheme

The FCT scheme in its original version [10] is by construction a new variant of a technique originally proposed by Boris and Book [6, 7, 8] in the context of fluid flow simulation. As shown in [10], the FCT scheme results in accurate

and (largely) rotationally invariant discrete representations of continuous-scale morphological dilation/erosion. For the sake of brevity we will not provide a derivation of the scalar FCT scheme since it can be found in detail in [10], see also [14] for its isotropic extension to matrix fields. We will also provide the directional modifications of the FCT method in the *two-dimensional* case only.

The basic idea of FCT is as follows. In a predictor step, the underlying PDE is solved by a simple and stable scheme usually afflicted with a fairly high diffusive numerical error. In a subsequent corrector step this error is negated by stabilised backward diffusion. The proposed FCT scheme relies on one-sided upwind differences as presented above. Using the Rouy-Tourin method as a *predictor*, denoting the result pointwise as  $u_{i,j}^{n+1,\text{pred}}$ , the FCT method relies on a *corrector step*, which will finally read as

$$u_{i,j}^{n+1} = u_{i,j}^{n+1,\text{pred}} + q_h^{n+1,\text{pred}} - q_d^{n+1,\text{pred}}. \quad (36)$$

One can identify the term  $q_h^{n+1,\text{pred}}$  in (36) as

$$q_h^{n+1,\text{pred}} := \left( \left( \frac{\tau}{h_x} \left| D_c^x u_{i,j}^{n+1,\text{pred}} \right| \right)^2 + \left( \frac{\tau}{h_y} \left| D_c^y u_{i,j}^{n+1,\text{pred}} \right| \right)^2 \right)^{1/2}. \quad (37)$$

For the term  $q_d^{n+1,\text{pred}}$  in (36) we make use of the quantities

$$g_{i+1/2,j} = \text{mm} \left( D_-^x u_{i,j}^{n+1,\text{pred}}, \frac{\tau}{2h_x} D_+^x u_{i,j}^{n+1,\text{pred}}, D_+^x u_{i+1,j}^{n+1,\text{pred}} \right) \quad (38)$$

$$g_{i,j+1/2} = \text{mm} \left( D_-^y u_{i,j}^{n+1,\text{pred}}, \frac{\tau}{2h_y} D_+^y u_{i,j}^{n+1,\text{pred}}, D_+^y u_{i,j+1}^{n+1,\text{pred}} \right) \quad (39)$$

where  $\text{mm}(\cdot, \cdot, \cdot)$  is the *scalar* minmod-function defined for three arguments as

$$\text{mm}(a_1, a_2, a_3) := \begin{cases} \inf(a_1, a_2, a_3) & \text{for } a_1, a_2, a_3 > 0, \\ \sup(a_1, a_2, a_3) & \text{for } a_1, a_2, a_3 < 0, \\ 0 & \text{else.} \end{cases} \quad (40)$$

With these abbreviations we set

$$\delta^x u_{i,j}^{n+1,\text{pred}} := \frac{\tau}{h_x} \left| D_c^x u_{i,j}^{n+1,\text{pred}} \right| + g_{i+1/2,j} - g_{i-1/2,j} \quad (41)$$

$$\delta^y u_{i,j}^{n+1,\text{pred}} := \frac{\tau}{h_y} \left| D_c^y u_{i,j}^{n+1,\text{pred}} \right| + g_{i,j+1/2} - g_{i,j-1/2} \quad (42)$$

which finally yields the second new term in (36) as

$$q_d^{n+1,\text{pred}} := \left( \left( \delta^x u_{i,j}^{n+1,\text{pred}} \right)^2 + \left( \delta^y u_{i,j}^{n+1,\text{pred}} \right)^2 \right)^{1/2}. \quad (43)$$

The directional version of the FCT-correction step (36) is now obtained by replacing the finite differences  $D_{(\cdot)}^x$  in  $x$ -direction in equations (37) to (43) by the weighted finite differences  $\|\nu\| D_{(\cdot)}^\nu$  in  $\nu$ -direction with  $\nu$  as in (3). We proceed in the same way with the other directions, substituting  $D_{(\cdot)}^y$  by  $\|\mu\| D_{(\cdot)}^\mu$ , and in the three-dimensional case, exchanging  $D_{(\cdot)}^z$  by  $\|\eta\| D_{(\cdot)}^\eta$ . Together with the directional Rouy-Tourin scheme we obtain the directional version of the FCT method which is used in this article.

The non-directional FCT method has been successfully transferred to the setting of matrix fields in [14]. So it is no surprise that the directional variant is readily extended to matrix fields. For details, especially concerning the matrix-valued counterpart of the minmod-function of three arguments by means of the Loewner ordering, the reader is referred to [14].

## 5 Morphological Operations

As indicated in the introduction the solution  $u$  of equation (1) mimics the dilation process with an adaptive ellipsoidal structuring element  $E$  which changes in time since it depends on  $u$ :  $E = E_u$ . Putting a minus sign on the right-hand-side of (1) gives the PDE-formulation of the corresponding adaptive erosion process. Using a common notation we express the dilation and the erosion of an original image  $f$  with such a structuring element  $E_u$  by

$$f \oplus E_u \quad \text{and} \quad f \ominus E_u . \quad (44)$$

The combinations of dilation and erosion lead to various morphological operators such as *opening* and *closing*,

$$f \circ E_u := (f \ominus E_u) \oplus E_u , \quad (45)$$

$$f \bullet E_u := (f \oplus E_u) \ominus E_u . \quad (46)$$

In an image, boundaries of objects are loci of high grey value variations, and as such they can be detected by derivative operators. The so-called *Beucher gradient*

$$\varrho_{E_u}(f) := (f \oplus E_u) - (f \ominus E_u) , \quad (47)$$

as well as the *internal* and *external gradient*,

$$\varrho_{E_u}^-(f) := f - (f \ominus E_u) , \quad \varrho_{E_u}^+(f) := (f \oplus E_u) - f , \quad (48)$$

are morphological counterparts of the norm of the gradient  $f$ ,  $\|\nabla f\|$ , if  $f$  is considered as a differentiable image.

In [47] a *morphological Laplacian* has been introduced. We define a variant by

$$\Delta_{E_u} f := \varrho_{E_u}^+(f) - \varrho_{E_u}^-(f) \quad (49)$$

$$= (f \oplus E_u) - 2 \cdot f + (f \ominus E_u). \quad (50)$$

This Laplacian is a morphological equivalent of the second derivative  $\partial_{\eta\eta} f$  where  $\eta$  stands for the unit vector in the direction of the steepest slope. It allows us to distinguish between influence zones of minima and maxima of the image  $f$ . This is a vital property for the construction of so-called shock filters [25, 27, 33]. Shock filtering amounts to applying either a dilation or an erosion to an image, depending on whether the pixel is located within the influence zone of a minimum or a maximum:

$$S_{E_u} f := \begin{cases} f \oplus E_u, & \Delta_{E_u} f < 0, \\ f, & \Delta_{E_u} f = 0, \\ f \ominus E_u, & \Delta_{E_u} f > 0. \end{cases} \quad (51)$$

A considerable number of variants of shock filters have been considered in the literature [2, 24, 32, 36, 39, 48]. When they are applied iteratively, experiments show that their steady state is given by a piecewise constant image with discontinuities (“shocks”) between adjacent segments of constant grey value. For more details about the morphological shock filter as introduced above, see [17].

In the experimental Section 6 we will see the results obtained by the various adaptive, PDE-driven morphological operators when applied to 2D and 3D matrix fields.

## 6 Experiments

The matrix data are visualised as an ellipsoid in each voxel via the level sets of quadratic form  $\{v \in \mathbb{R}^3 v : v^\top U^{-2}(i, j, k)v = \text{const.}\}$ . It is associated with the matrix  $U(i, j, k) \in \text{Sym}_3^+(\mathbb{R})$  representing the matrix field at voxel  $(ih_x, jh_y, kh_z)$ . By using  $U^{-2}$  the length of the semi-axes of the ellipsoid correspond directly with the three eigenvalues of the matrix. Changing the constant *const.* amounts to a mere scaling of the ellipsoids. Note that only positive definite matrices produce ellipsoids as level sets of its quadratic form. In the following we employ the Rouy-Tourin scheme, the FCT scheme, and their corresponding directional versions. In all schemes we use a grid size  $h_x = h_y = h_z = 1$ .

## 6.1 Synthetic data in 2D and 3D

Figure 1(a) exhibits a  $32 \times 32$  matrix field composed of two interrupted diagonal stripes with different thickness, both built with cigar-shaped ellipsoids of equal size but different orientation. The line-like structures are tilted with respect to the  $x$ -axis by an angle of about 117 degrees. Figure 1(b) shows the result of applying coherence-enhancing diffusion (CED) [19]. Figure 1(c) contains the result of isotropic (classical) dilation [16] using the Rouy-Tourin scheme, and Figure 1(d) the result of the proposed adaptive anisotropic dilation after applying the directional Rouy-Tourin scheme. The parameters used were chosen in a way that every method fills in the missing tensors of both stripes. Our approach is able to complete the line-like structures much faster and more accurate than the other methods. Moreover, note that the direction and amount of adaptive anisotropic dilation does not depend on the orientation of the ellipsoids, but on the orientation and width of the structures. It is worth mentioning that the CED approach decreases the overall size of matrices since the total mass, that is, the volume of the ellipsoids is only redistributed due to the property of mass conservation. The same experiment is performed on a 2D spiral data set with missing information, whose outcome is depicted in Figure 2. Again, only the directional dilation succeeds to close the gaps satisfactorily preserving the spiral structure of the object. As expected, the adaptive dilation process is faster than the diffusion based method and the classical isotropic dilation.

We now use both the *directional* Rouy-Tourin scheme and the *directional* FCT scheme for dilating the test image with an interrupted circular structure shown at the top of Figure 3. In the first test the dilation process is steered in tangential direction while in a second test the radial direction is selected via the choice of the parameter  $c = (c_1, c_2)$ , namely  $c = (0.1, 10)$  in the first case and  $c = (10, 0.1)$  in the second one. Both directional schemes were applied, the results together with a scaled ( $\times 5$ ) absolute difference image are depicted in Figure 3. As expected the directional FCT method performs favourable in terms of edge preservation over the directional Rouy-Tourin scheme.

A much more elaborate matrix field can be seen in Figure 4(a). This 3D data set<sup>2</sup> is sparsified by removing 80% of the matrices (Figure 4(b)). Both adaptive anisotropic dilation (Figure 4(c)) and closing (Figure 4(d)) performed with the superior *directional* FCT scheme, provide a reasonable reconstruction of the original data.

---

<sup>2</sup>The 3D spiral data set is freely available as part of the Teem toolkit at <http://teem.sourceforge.net>.

## 6.2 Real world data: 3D DT-MRI

We also tested the proposed method on a real DT-MRI data set of a human head consisting of a  $128 \times 128 \times 38$ -field of positive definite matrices. Figure 5(a) displays part of the lateral ventricles as an actual three-dimensional  $40 \times 55 \times 3$ -data set while Figure 5(b) shows only a 2D-slice. In the experiments on real-world data we will always juxtapose the results of various adaptive morphological operations when applied to 2D-slices and truly 3D data. However, in order to avoid visual cluttering, we will in general extract and depict from the processed 3D data an appropriate 2D-slice only. Note that we use for the adaptive morphological operations from now on only the directional FCT scheme in its 3D and 2D realisations.

In Figure 6 we zoom into the lateral ventricles to show the effect of applying adaptive dilation and erosion in both the 3D and 2D setting. We see that the adaptive dilation and erosion processes on matrix fields respect the underlying shape of the ventricles if compared to the isotropic case [14]. We notice that the results are quite similar in the 3D and in the 2D setting. However, the 3D process seems to be more accurate at the price of a longer evolution time ( $t = 3$ ), than in the 2D case ( $t = 1$ ).

The lateral ventricles serve also as a test case for the reconstructing operations of adaptive opening and closing, Figure 7. In 3D the lateral ventricles are nicely recovered in a slightly simplified form, as expected, since it incorporates also information from neighbouring slices.

The difference in processing of 2D and 3D data sets becomes prominent in the case of the morphological derivatives, e.g. the Beucher gradient. The gradient operations detect the boundary of the ventricles, which are three-dimensional anatomical structures. This boundary in a cross-section can be seen clearly in Figure 8(a). In contrast to this, the boundaries are less localised in the 2D case, Figure 8(b).

For the adaptive version of the morphological shock filter we obtain the matrix valued equivalent of a piece-wise constant image both in the 3D and the 2D case. In the three-dimensional setting, Figure 8(c), we observe a slightly better localisation of the shock segments than in 2D, Figure 8(d).

## 7 Conclusion

We have presented a method for an adaptive, PDE-based dilation and erosion processes in the setting of matrix fields. The evolution governed by matrix-valued PDEs is guided by a steering tensor whose construction relies on the full structure tensor for matrix data.

In order to enable proper directional steering we extended the schemes of Rouy-Tourin and the FCT method in two ways: First, turning them into directional schemes based on directional finite differences via interpolation. Second, by means of advanced matrix calculus, extending these directional variants to matrix fields solving the matrix-valued adaptive PDEs of dilation and erosion. Having these two key operations at our disposal we were able to propose higher order morphological operators such as top hats and morphological derivatives that are adaptive and act on matrix fields.

As a proof-of-concept we applied these adaptive morphological operations to synthetic and real DT-MRI data. The tests reveal that the various adaptive morphological operators behave as one might expected from their scalar counterparts. For instance, the adaptive dilation and closing are indeed capable of filling in missing data and to complete directional structures. We also confirmed that the FCT performs preferable over the scheme of Rouy and Tourin.

The proposed approach to adaptive morphology for matrix fields may have its merits, for example, in the segmentation of directional structures or as a preprocessing step for fiber tracking algorithms in medical imaging.

### **Acknowledgements.**

We gratefully acknowledge partial funding by the *Deutscher Akademischer Austauschdienst* (DAAD), grant A/05/21715, for the second author.

The DT-MRI data set has been provided by Anna Vilanova i Bartoli, Eindhoven University of Technology.

We thank Thomas Schultz (Max-Planck Institute for Computer Science) for his help in formatting the 3D spiral data set.

## **References**

- [1] L. Alvarez, F. Guichard, P.-L. Lions, and J.-M. Morel. Axioms and fundamental equations in image processing. *Archive for Rational Mechanics and Analysis*, 123:199–257, 1993.
- [2] L. Alvarez and L. Mazorra. Signal and image restoration using shock filters and anisotropic diffusion. *SIAM Journal on Numerical Analysis*, 31:590–605, 1994.
- [3] A. B. Arehart, L. Vincent, and B. B. Kimia. Mathematical morphology: The Hamilton–Jacobi connection. In *Proc. Fourth International Conference on Computer Vision*, pages 215–219, Berlin, May 1993. IEEE Computer Society Press.

- [4] J. Bigün. *Vision with Direction*. Springer, Berlin, 2006.
- [5] J. Bigün, G. H. Granlund, and J. Wiklund. Multidimensional orientation estimation with applications to texture analysis and optical flow. *IEEE Transactions on Pattern Analysis and Machine Intelligence*, 13(8):775–790, August 1991.
- [6] J. P. Boris and D. L. Book. Flux corrected transport. I. SHASTA, a fluid transport algorithm that works. *Journal of Computational Physics*, 11(1):38–69, 1973.
- [7] J. P. Boris and D. L. Book. Flux corrected transport. III. Minimal error FCT algorithms. *Journal of Computational Physics*, 20:397–431, 1976.
- [8] J. P. Boris, D. L. Book, and K. Hain. Flux corrected transport. II. Generalizations of the method. *Journal of Computational Physics*, 18:248–283, 1975.
- [9] M. Breuß, B. Burgeth, and J. Weickert. Anisotropic continuous-scale morphology. In J. Martí, J. M. Benedí, A. M. Mendonça, and J. Serrat, editors, *Pattern Recognition and Image Analysis*, volume 4478 of *Lecture Notes in Computer Science*, pages 515–522. Springer, Berlin, 2007.
- [10] M. Breuß and J. Weickert. A shock-capturing algorithm for the differential equations of dilation and erosion. *Journal of Mathematical Imaging and Vision*, 25(2):187–201, September 2006.
- [11] M. Breuß and J. Weickert. Highly accurate PDE-based morphology for general structuring elements. In X.-C. Tai et al., editor, *Proc. of the Second International Conference on Scale Space and Variational Methods in Computer Vision*, volume 5567 of *Lecture Notes in Computer Science*, pages 758–769. Springer, Berlin, 2009.
- [12] R. W. Brockett and P. Maragos. Evolution equations for continuous-scale morphological filtering. *IEEE Transactions on Signal Processing*, 42:3377–3386, 1994.
- [13] T. Brox, J. Weickert, B. Burgeth, and P. Mrázek. Nonlinear structure tensors. *Image and Vision Computing*, 24(1):41–55, January 2006.
- [14] B. Burgeth, M. Breuß, S. Didas, and J. Weickert. PDE-based morphology for matrix fields: Numerical solution schemes. In S. Aja-Fernández, R. de Luis García, D. Tao, and X. Li, editors, *Tensors in Image Processing and Computer Vision*, Advances in Pattern Recognition, pages 125–150. Springer, London, 2009.

- [15] B. Burgeth, M. Breuß, L. Pizarro, and J. Weickert. PDE-driven adaptive morphology for matrix fields. In X.-C. Tai et al., editor, *Proc. of the Second International Conference on Scale Space and Variational Methods in Computer Vision*, volume 5567 of *Lecture Notes in Computer Science*, pages 247–258. Springer, Berlin, 2009.
- [16] B. Burgeth, A. Bruhn, S. Didas, J. Weickert, and M. Welk. Morphology for matrix-data: Ordering versus PDE-based approach. *Image and Vision Computing*, 25(4):496–511, 2007.
- [17] B. Burgeth, A. Bruhn, N. Papenberg, M. Welk, and J. Weickert. Mathematical morphology for tensor data induced by the Loewner ordering in higher dimensions. *Signal Processing*, 87(2):277–290, February 2007.
- [18] B. Burgeth, S. Didas, L. Florack, and J. Weickert. A generic approach to diffusion filtering of matrix-fields. *Computing*, 81:179–197, 2007.
- [19] B. Burgeth, S. Didas, and J. Weickert. A general structure tensor concept and coherence-enhancing diffusion filtering for matrix fields. In D. Laidlaw and J. Weickert, editors, *Visualization and Processing of Tensor Fields*, Mathematics and Visualization, pages 305–323. Springer, Berlin, 2009.
- [20] C. Ched’Hotel, D. Tschumperlé, R. Deriche, and O. Faugeras. Constrained flows of matrix-valued functions: Application to diffusion tensor regularization. In A. Heyden, G. Sparr, M. Nielsen, and P. Johansen, editors, *Computer Vision – ECCV 2002*, volume 2350 of *Lecture Notes in Computer Science*, pages 251–265. Springer, Berlin, 2002.
- [21] S. Di Zenzo. A note on the gradient of a multi-image. *Computer Vision, Graphics and Image Processing*, 33:116–125, 1986.
- [22] C. Feddern, J. Weickert, B. Burgeth, and M. Welk. Curvature-driven PDE methods for matrix-valued images. *International Journal of Computer Vision*, 69(1):91–103, August 2006.
- [23] W. Förstner and E. Gülch. A fast operator for detection and precise location of distinct points, corners and centres of circular features. In *Proc. ISPRS Intercommission Conference on Fast Processing of Photogrammetric Data*, pages 281–305, Interlaken, Switzerland, June 1987.
- [24] G. Gilboa, N. A. Sochen, and Y. Y. Zeevi. Regularized shock filters and complex diffusion. In A. Heyden, G. Sparr, M. Nielsen, and P. Johansen,

- editors, *Computer Vision – ECCV 2002*, volume 2350 of *Lecture Notes in Computer Science*, pages 399–413. Springer, Berlin, 2002.
- [25] F. Guichard and J.-M. Morel. A note on two classical enhancement filters and their associated PDE’s. *International Journal of Computer Vision*, 52(2/3):153–160, 2003.
- [26] R. A. Horn and C. R. Johnson. *Matrix Analysis*. Cambridge University Press, Cambridge, UK, 1990.
- [27] H. P. Kramer and J. B. Bruckner. Iterations of a non-linear transformation for enhancement of digital images. *Pattern Recognition*, 7:53–58, 1975.
- [28] D. Laidlaw and J. Weickert, editors. *Visualization and Processing of Tensor Fields*. Springer, Berlin, 2009.
- [29] G. Matheron. *Éléments pour une théorie des milieux poreux*. Masson, Paris, 1967.
- [30] G. Matheron. *Random Sets and Integral Geometry*. Wiley, New York, 1975.
- [31] S. Osher and R. P. Fedkiw. *Level Set Methods and Dynamic Implicit Surfaces*, volume 153 of *Applied Mathematical Sciences*. Springer, New York, 2002.
- [32] S. Osher and L. Rudin. Shocks and other nonlinear filtering applied to image processing. In A. G. Tescher, editor, *Applications of Digital Image Processing XIV*, volume 1567 of *Proceedings of SPIE*, pages 414–431. SPIE Press, Bellingham, 1991.
- [33] S. Osher and L. I. Rudin. Feature-oriented image enhancement using shock filters. *SIAM Journal on Numerical Analysis*, 27:919–940, 1990.
- [34] S. Osher and J. A. Sethian. Fronts propagating with curvature-dependent speed: Algorithms based on Hamilton–Jacobi formulations. *Journal of Computational Physics*, 79:12–49, 1988.
- [35] L. Pizarro, B. Burgeth, M. Breuß, and J. Weickert. A directional Rouy–Tourin scheme for adaptive matrix-valued morphology. In *Proc. of the Ninth International Symposium on Mathematical Morphology (ISMM 2009)*, 2009. Accepted for publication.

- [36] L. Remaki and M. Cheriet. Numerical schemes of shock filter models for image enhancement and restoration. *Journal of Mathematical Imaging and Vision*, 18(2):153–160, March 2003.
- [37] E. Rouy and A. Tourin. A viscosity solutions approach to shape-from-shading. *SIAM Journal on Numerical Analysis*, 29:867–884, 1992.
- [38] G. Sapiro, R. Kimmel, D. Shaked, B. B. Kimia, and A. M. Bruckstein. Implementing continuous-scale morphology via curve evolution. *Pattern Recognition*, 26:1363–1372, 1993.
- [39] J. G. M. Schavemaker, M. J. T. Reinders, and R. van den Boomgaard. Image sharpening by morphological filtering. In *Proc. 1997 IEEE Workshop on Nonlinear Signal and Image Processing*, Mackinac Island, MI, September 1997. [www.ecn.purdue.edu/NSIP/](http://www.ecn.purdue.edu/NSIP/).
- [40] J. Serra. *Echantillonnage et estimation des phénomènes de transition minier*. PhD thesis, University of Nancy, France, 1967.
- [41] J. Serra. *Image Analysis and Mathematical Morphology*, volume 1. Academic Press, London, 1982.
- [42] J. Serra. *Image Analysis and Mathematical Morphology*, volume 2. Academic Press, London, 1988.
- [43] J. A. Sethian. *Level Set Methods and Fast Marching Methods*. Cambridge University Press, Cambridge, UK, second edition, 1999. Paperback edition.
- [44] P. Soille. *Morphological Image Analysis*. Springer, Berlin, second edition, 2003.
- [45] R. van den Boomgaard. *Mathematical Morphology: Extensions Towards Computer Vision*. PhD thesis, University of Amsterdam, The Netherlands, 1992.
- [46] R. van den Boomgaard. Numerical solution schemes for continuous-scale morphology. In M. Nielsen, P. Johansen, O. F. Olsen, and J. Weickert, editors, *Scale-Space Theories in Computer Vision*, volume 1682 of *Lecture Notes in Computer Science*, pages 199–210. Springer, Berlin, 1999.
- [47] L. J. van Vliet, I. T. Young, and A. L. D. Beckers. A nonlinear Laplace operator as edge detector in noisy images. *Computer Vision, Graphics and Image Processing*, 45(2):167–195, 1989.

- [48] J. Weickert. Coherence-enhancing shock filters. In B. Michaelis and G. Krell, editors, *Pattern Recognition*, volume 2781 of *Lecture Notes in Computer Science*, pages 1–8. Springer, Berlin, 2003.
- [49] J. Weickert and T. Brox. Diffusion and regularization of vector- and matrix-valued images. In M. Z. Nashed and O. Scherzer, editors, *Inverse Problems, Image Analysis, and Medical Imaging*, volume 313 of *Contemporary Mathematics*, pages 251–268. AMS, Providence, 2002.
- [50] J. Weickert and H. Hagen, editors. *Visualization and Processing of Tensor Fields*. Springer, Berlin, 2006.

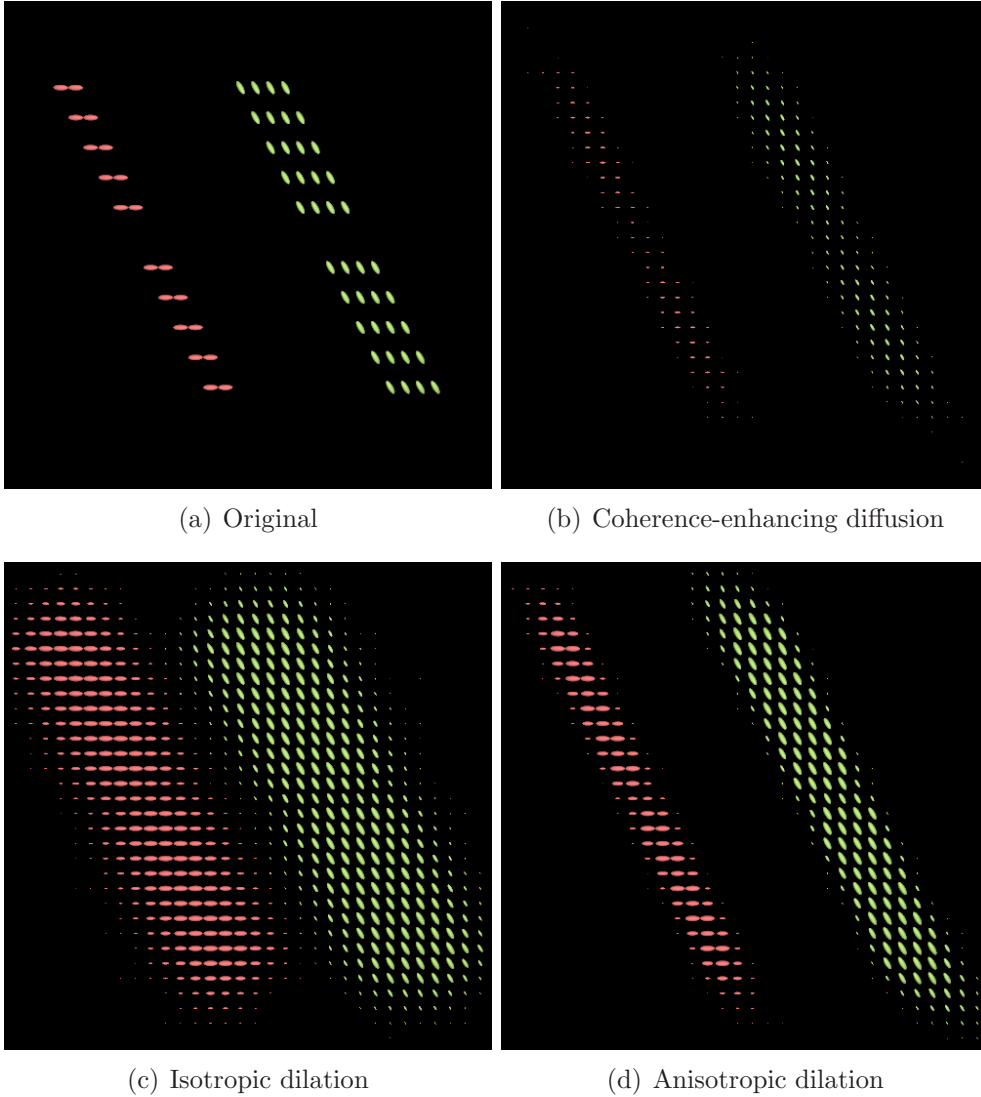


Figure 1: Comparison of different methods in 2D. (a) Original matrix field with ellipsoids in a line-like arrangement. (b) Coherence-enhancing diffusion (CED) with  $\rho = 4, t = 3$ . (c) Isotropic (classical) dilation at  $t = 3$  using the Rouy-Tourin scheme. (d) Proposed adaptive, anisotropic dilation using the *directional* Rouy-Tourin scheme with  $\rho = 4, c = (0.2, 20), t = 1$ .

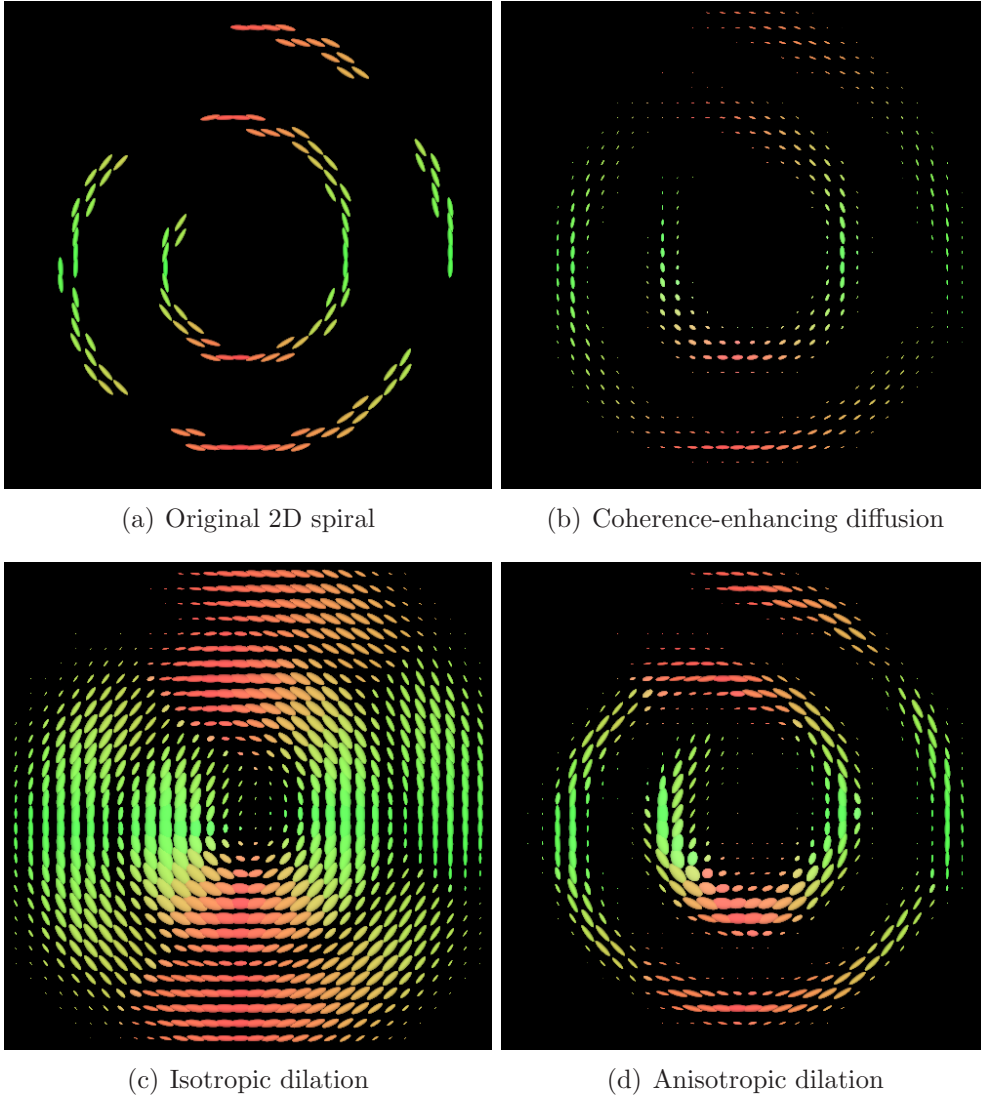


Figure 2: Comparison of different methods in 2D. (a) Original spiral with missing tensors. (b) Coherence-enhancing diffusion (CED) with  $\rho = 3, t = 6$ . (c) Isotropic dilation at  $t = 3$  using the Rouy-Tourin scheme. (d) Proposed adaptive, anisotropic dilation using the *directional* Rouy-Tourin scheme with  $\rho = 3, c = (0.2, 20), t = 1$ .

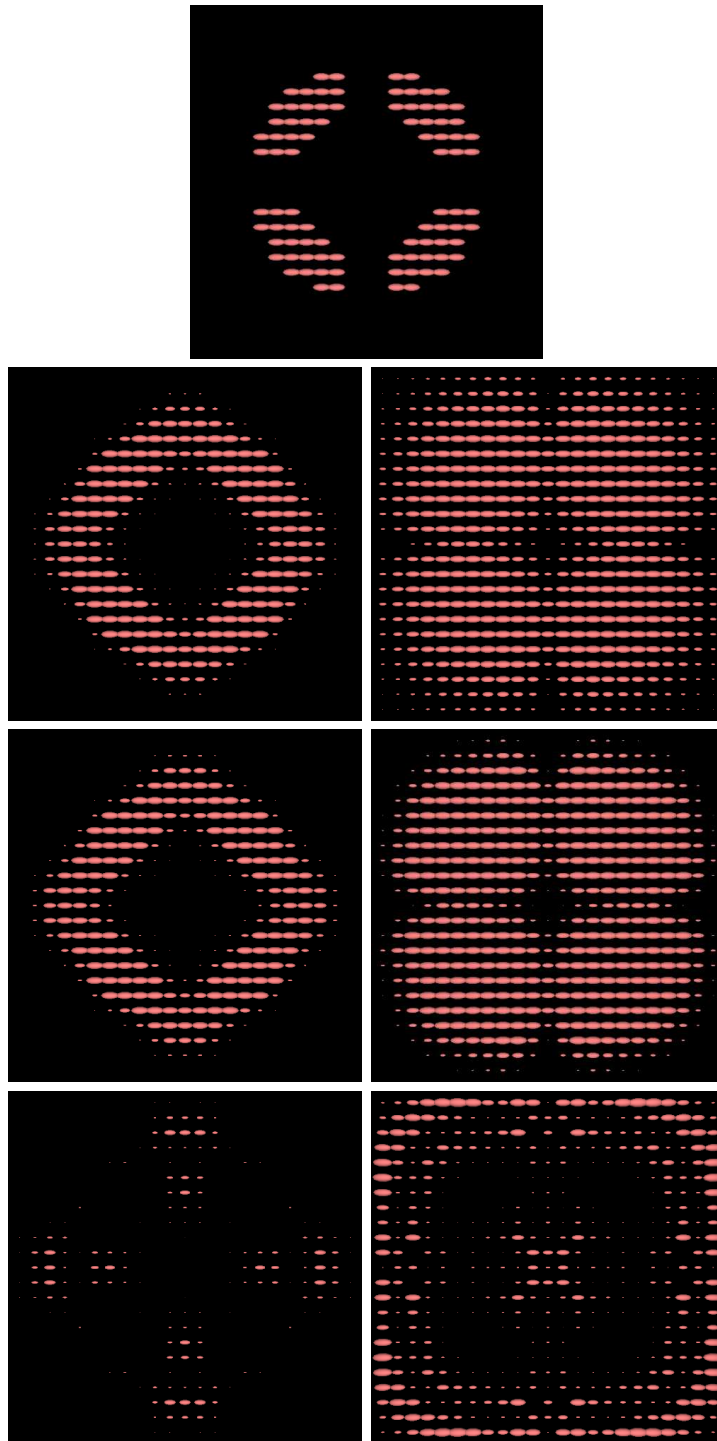
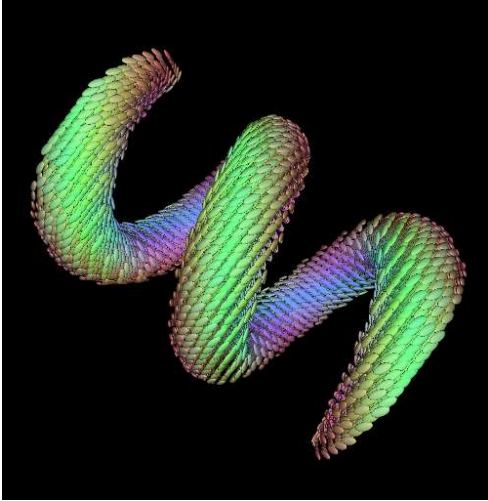
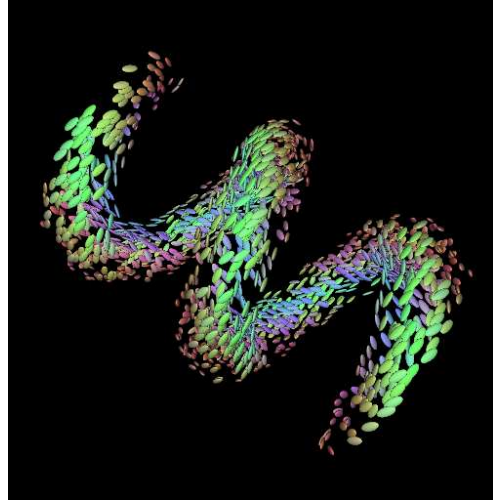


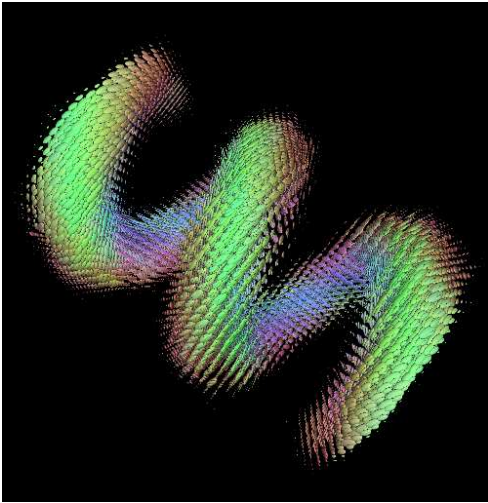
Figure 3: **Top row:** Synthetic 2D circle with missing information. **Second row:** From left to right: Dilation with *directional* Rouy-Tourin scheme in the tangential direction and in the radial direction. **Third row:** The same using the *directional* FCT scheme. **Bottom row:** Scaled absolute differences between both schemes.



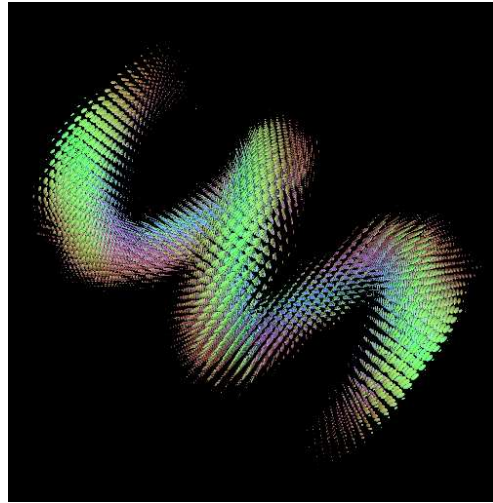
(a) Original 3D spiral



(b) Sampled spiral (20%)

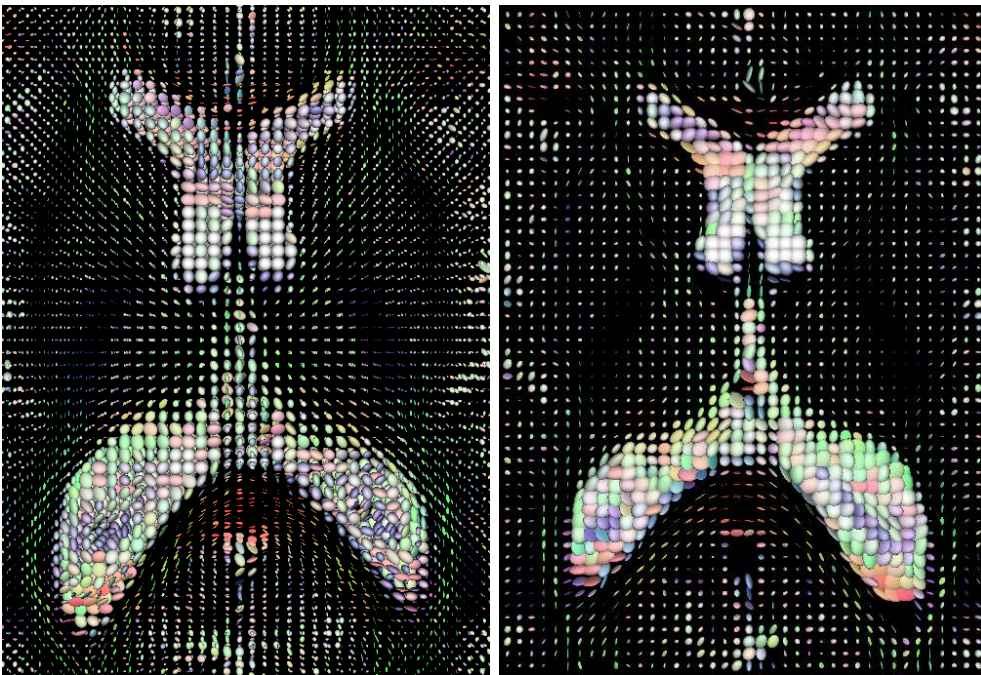


(c) Anisotropic dilation of (b)



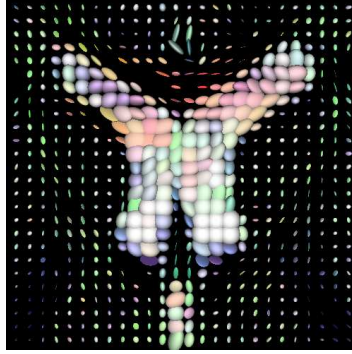
(d) Anisotropic closing of (b)

Figure 4: Adaptive, anisotropic dilation and closing in 3D using the *directional* FCT scheme with parameters  $\rho = 2, c = (0.2, 0.2, 20), t = 5$ .

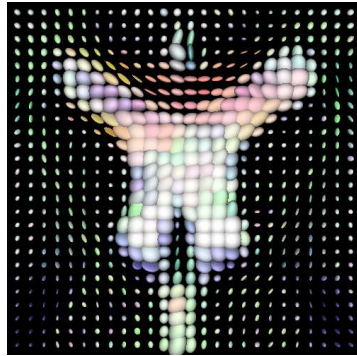


(a) Original 3D section of DT-MRI data      (b) 2D slice with  $40 \times 55$  matrices

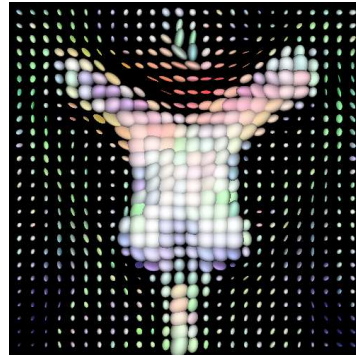
Figure 5: Real world data used in our experiments.



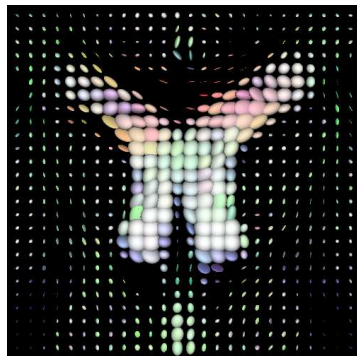
(a) Original



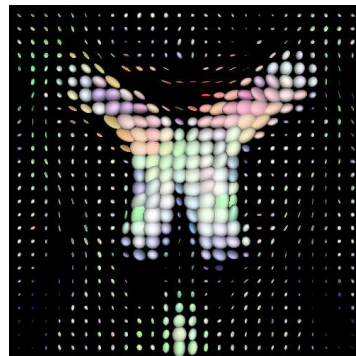
(b) 3D dilation



(c) 2D dilation

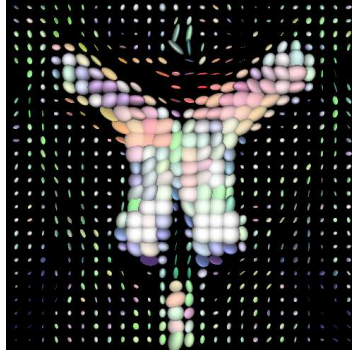


(d) 3D erosion

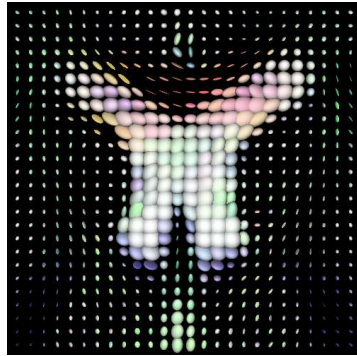


(e) 2D erosion

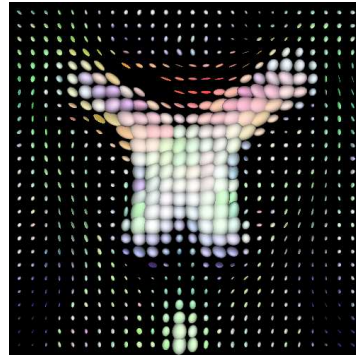
Figure 6: Adaptive, anisotropic dilation and erosion in 3D and 2D using the *directional* FCT scheme with parameters  $\rho = 1, c = (0.05, 0.05, 5), t = 3$  in the 3D case, and  $\rho = 1, c = (0.05, 5), t = 1$  in the 2D case.



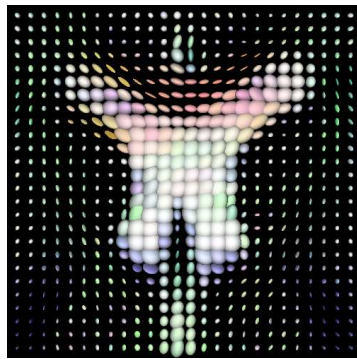
(a) Original



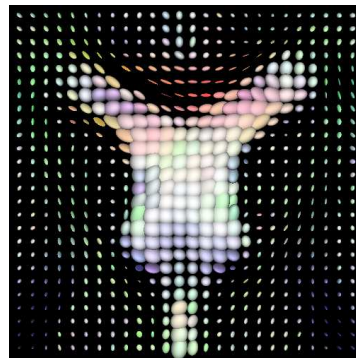
(b) 3D opening



(c) 2D opening

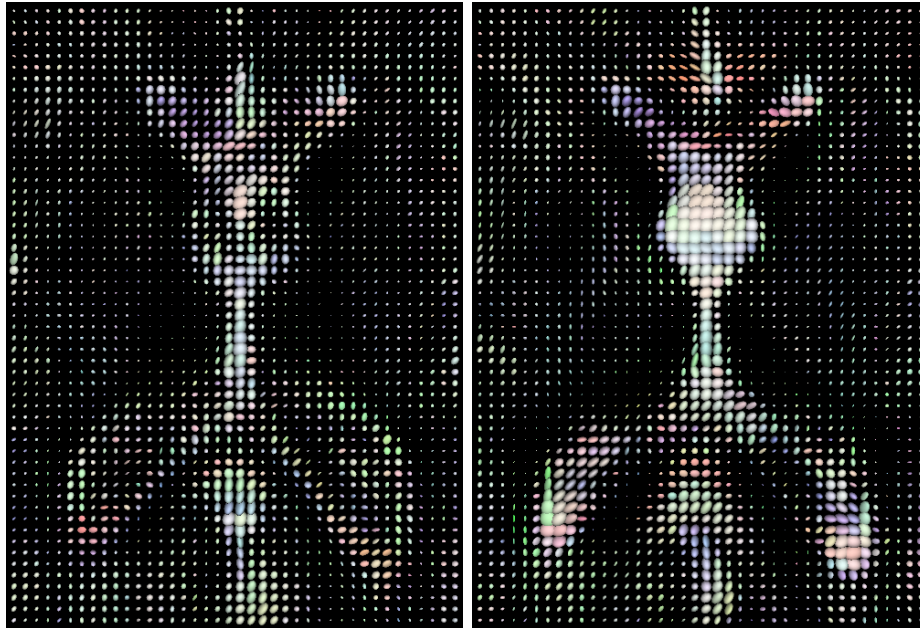


(d) 3D closing



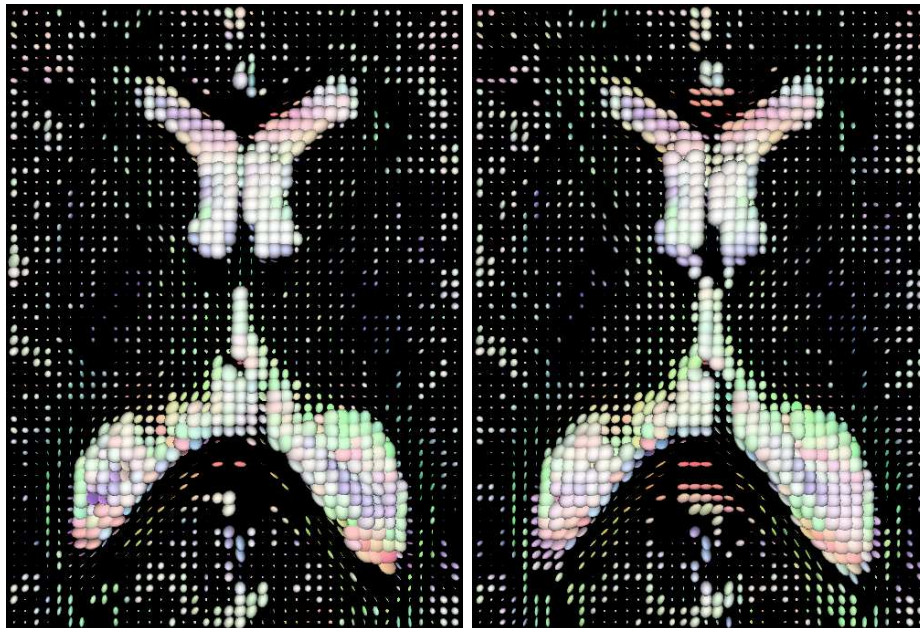
(e) 2D closing

Figure 7: Adaptive, anisotropic opening and closing in 3D and 2D using the *directional* FCT scheme with parameters  $\rho = 1, c = (0.05, 0.05, 5), t = 3$  in the 3D case, and  $\rho = 1, c = (0.05, 5), t = 1$  in the 2D case.



(a) 3D Beucher gradient

(b) 2D Beucher gradient



(c) 3D shock filtering

(d) 2D shock filtering

Figure 8: Adaptive, anisotropic Beucher gradient and shock filtering in 3D and 2D using the *directional* FCT scheme with parameters  $\rho = 1, c = (0.1, 0.1, 10), t = 5$  in the 3D case, and  $\rho = 1, c = (0.1, 10), t = 2$  in the 2D case.